Available online at www.sciencedirect.com
SCIENCE DIRECT®
Journal of Sound and Vibration 285 (2005) 1180–1188
JOURNAL OF SOUND AND VIBRATION
www.elsevier.com/locate/jsvi

Short Communication

A hydro-mechanical model for hysteretic damping force prediction of ER damper: experimental verification

S.R. Hong[a], S.B. Choi[a,*], Y.T. Choi[b], N.M. Wereley[b]

[a]*Smart Structures and Systems Laboratory, Department of Mechanical Engineering, Inha University, 253 Yong Hyun-Dong, Nam-Gu, Incheon 402-751, Korea*
[b]*Smart Structures Laboratory, Department of Aerospace Engineering, University of Maryland, College Park, MD 20742, USA*

Received 1 March 2004; received in revised form 16 August 2004; accepted 25 October 2004
Available online 22 December 2004

Abstract

This paper presents a hydro-mechanical model for hysteretic damping force prediction of an electrorheological (ER) damper which can be applicable to a small-sized passenger vehicle. A mathematical model which well describes physical flow motion of the hydraulic system is formulated. Then, a cylindrical type of ER damper is devised and its hysteretic behavior is empirically evaluated in the damping force versus piston velocity domain. The measured damping characteristics are compared with those predicted from the proposed hydro-mechanical model. In addition, the averaged error between the predicted and measured damping force is calculated in order to evaluate the model accuracy.

1. Introduction

Electrorheological (ER) and magnetorheological (MR) dampers have been proposed for vibration attenuation of various dynamic systems including vehicle suspensions. It has been demonstrated via experimental realization that unwanted vibrations of application systems can be effectively controlled by employing semi-active ER or MR dampers [1–4]. In order to achieve

*Corresponding author. Tel.: +82 32 860 7319; fax: +82 32 868 1716.
E-mail address: seungbok@inha.ac.kr (S.B. Choi).

0022-460X/$ - see front matter © 2004 Elsevier Ltd. All rights reserved.
doi:10.1016/j.jsv.2004.10.031

desirable control performance, it is necessary to have an accurate damping force model which can capture the inherent hysteresis behavior of ER or MR damper. So far, several types of damper models have been proposed and used to describe the damping force behavior of ER or MR damper. The simple Bingham model [5,6] gives a good description of post-yield force behavior of ER or MR damper, but the transition from pre-yield to post-yield is discontinuous and the hysteretic behavior cannot be described. The hysteretic Bingham plastic model [4], the hysteretic biviscous model [7,8], the nonlinear viscoelastic plastic model [9], the Bouc–Wen model [10,11], the polynomial model [12] are effective models for prediction of the field-dependent hysteretic damping force of ER or MR dampers. However, these models do not describe the flow motion of the damper, which is inherent feature in hydraulic damper mechanism.

Consequently, the main contribution of this work is to propose a hysteresis damper model which can describe the flow motion of the hydraulic system. In order to achieve the goal, a cylindrical type of ER damper, which can be applicable to a small-sized passenger vehicle, is adopted and its hysteretic behavior is experimentally evaluated in the damping force versus piston velocity domain. The measured hysteresis characteristics of the field-dependent damping forces are compared with those predicted from the models; simple Bingham model and the proposed hydro-mechanical model. In addition, the averaged error between the predicted and measured force is calculated in order to evaluate the model accuracy.

2. ER damper

The schematic configuration of a flow-mode ER damper tested in this study is shown in Fig. 1. The ER damper consists of hydraulic and pneumatic reservoirs separated by a floating piston. Inside of the hydraulic reservoir, the piston rod is attached to a piston head. During the piston

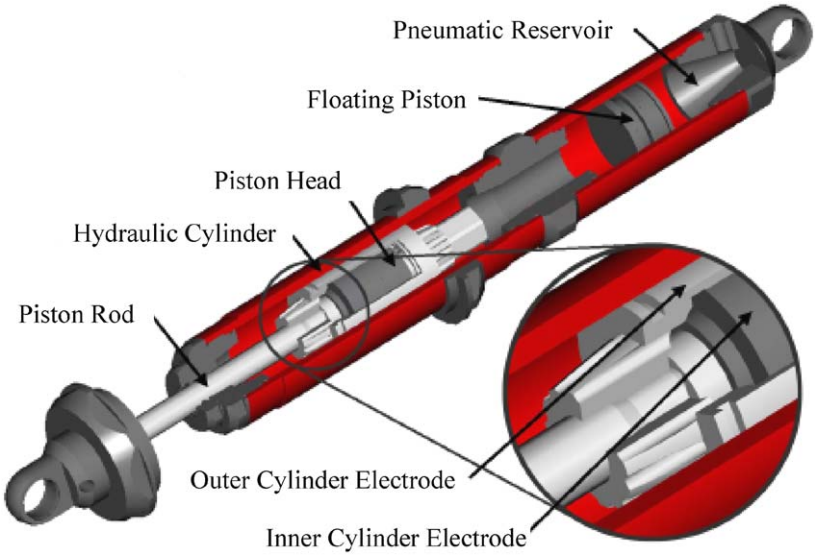

Fig. 1. Configuration of the ER damper.

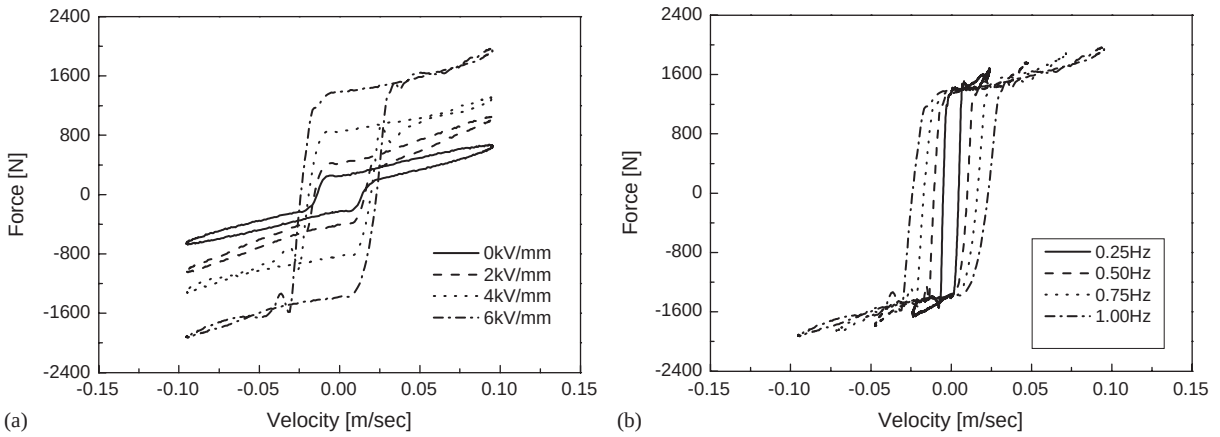

Fig. 2. Measured damping force characteristics. (a) Force vs. velocity cycles for 1.0 Hz excitation and various electric fields, (b) force vs. velocity cycles for 6.0 kV/mm and various excitation frequencies.

motion, ER fluid flows through a gap between inner and outer cylinder electrodes in the piston head and can be energized by applied electric fields. The principal design parameters are chosen as follows: electrode length is 43 mm and electrode gap is 0.65 mm. On the other hand, the composition ratio of the ER fluid employed in this study is 40% corn starch and 60% peanut oil by weight. Nitrogen-filled pneumatic reservoir and floating piston located inside of the hydraulic cylinder are used to prevent cavitation on the low-pressure side of the piston and accumulate the ER fluid induced by the motion of the piston. In order to measure the field-dependent damping force of the ER damper, a hydraulic excitation system has been used [2,3,5]. The sinusoidal excitation was applied with the magnitude of 12.7 mm.

Fig. 2(a) presents the measured damping force characteristics at the excitation frequency of 1.0 Hz. As the applied electric field increases, the damping force also increases due to the increment of yield stress of ER fluid under flow mode operation. We can see the Bingham-like behavior which consists of the viscous damping force and field-dependent yield force in the high-velocity region. In the low-velocity region, we can clearly observe the hysteresis loop. As the electric field increases, the width of the hysteresis loop is enlarged and its slope increases. The hysteresis loop at 0 kV/mm is mainly due to the frictional force of the seal components and compliance effect inside the ER damper. This frictional force behaves as the field-dependent yield force. When the electric field is applied to the electrodes, the sum of the field-dependent yield force and frictional force affects the hysteresis behavior of ER damper. Fig. 2(b) shows the damping force vs. velocity cycles with different excitation frequencies for the electric field of 6 kV/mm. For higher excitation frequencies, the hysteresis loop widens and the hysteresis slope decreases.

3. Hydro-mechanical model

As a comparative model, the Bingham model is firstly introduced. In Bingham model, the yield stress (τ_y) of the ER fluid is described by

$$\tau_y = \alpha E^{\beta} \tag{1}$$

where E is the electric field, α and β are intrinsic values of the ER fluid which are to be experimentally identified. Thus, the damping fore of the ER damper can be obtained [3] by

$$F = c_0 v + \alpha_1 \alpha E^{\beta} \operatorname{sgn}(v) \tag{2}$$

In the above equation, v is the piston velocity, c_0 the damping constant due to the viscosity of the ER fluid, and α_1 the geometrical constant. The second term is, of course, the controllable damping force by input electric field of E.

A schematic configuration of the hydro-mechanical model proposed in this work is shown in Fig. 3(a). Control volume of the electrode gap (#3) is lumped into the fluid inertance I_f and zero-field flow resistance R_f. On the other hand, ΔP_{ER} is the pressure drop due to the yield stress of ER fluid. Control volumes of lower, upper, and gas chambers (#1, #2, and #4) are represented by the compliances C_1, C_2, and C_4, respectively. From the hydraulic model shown in Fig. 3(a), the total pressure drop due to the ER fluid passing through the electrode gap can be given by

$$\Delta P = P_2 - P_1 = I_f A_f \ddot{x}_r + R_f A_f \dot{x}_r + \Delta P_{\mathrm{ER}} \operatorname{sgn}(\dot{x}_r) \tag{3}$$

where

$$I_f = \frac{\rho l}{A_f}, \quad R_f = \frac{12\eta l}{b h^3}, \quad \Delta P_{\mathrm{ER}} = 2\,\frac{l}{h}\,\tau_y(E), \quad x_r = x_f - x \tag{4}$$

In the above, ΔP is the pressure difference between upper and lower chambers, P_1 the pressure of the lower chamber, P_2 the pressure of the upper chamber, ΔP_{ER} the pressure drop due to the electric field, x_f the displacement of fluid inertance, and x_r the relative displacement of fluid inertance, and x the piston displacement. Here, ρ and η are the density and the zero-field viscosity of the employed ER fluid, respectively. Geometric parameters are as follows: l the electrode length, h the electrode gap size, b the electrode gap width, and A_f the cross-sectional area of the electrode gap. By applying continuity augments to the lower and upper chambers, gas chamber

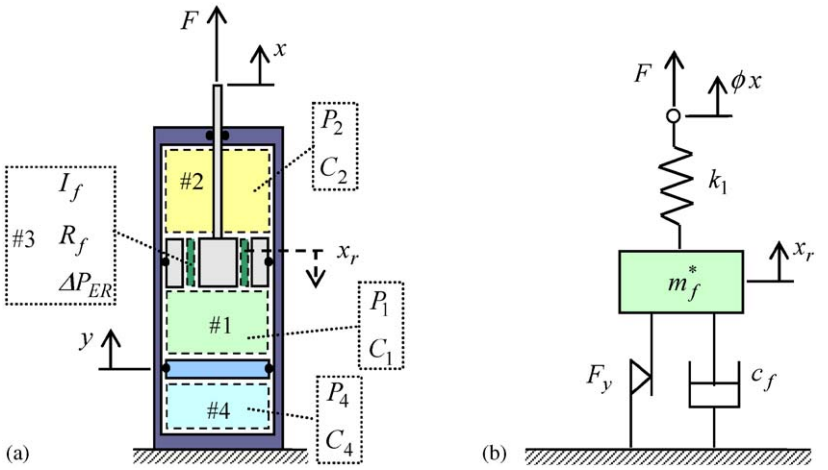

Fig. 3. Mathematic model of the ER damper. (a) Hydro-mechanical model, (b) analogous mechanical model.

and electrode duct, the followings equations are obtained [13]:

$$C_1\dot{P}_1 = -(A_1 - A_f)\dot{x} - A_f\dot{x}_r + A_4\dot{y} \tag{5}$$

$$C_2\dot{P}_2 = (A_2 - A_f)\dot{x} + A_f\dot{x}_r \tag{6}$$

$$C_4\dot{P}_4 = -A_4\dot{y} \tag{7}$$

where A_1, A_2, and A_4 are piston areas of lower, upper, and gas chambers, y the displacement of the floating-piston in the gas chamber, and $P_4(\approx P_1)$ the pressure of the gas chamber. By eliminating the internal variables P_1, P_2, P_4, and y from of Eqs. (3), (5)–(7), dynamic equations for the damping force are obtained as follows:

$$F = A_p\Delta P = m_f^*\ddot{x}_r + c_f\dot{x}_r + F_y\,\mathrm{sgn}(\dot{x}_r) \tag{8}$$

$$m_f^*\ddot{x}_r + c_f\dot{x}_r + F_y\,\mathrm{sgn}(\dot{x}_r) + k_1x_r = k_2x = k_1\Phi x \tag{9}$$

where

$$A_p \approx \frac{A_1 + A_2}{2},\ \ m_f^* = m_f \cdot \mu = I_f A_f A_p \cdot \mu,\ \ c_f = R_f A_f A_p,\ \ F_y = A_p\Delta P_{\mathrm{ER}} \tag{10}$$

$$\Phi = \frac{k_2}{k_1},\ \ k_1 = A_p(A_2 - A_f)\left(\frac{1}{C_1 + C_4} + \frac{1}{C_2}\right),\ \ k_2 = A_pA_f\left(\frac{1}{C_1 + C_4} + \frac{1}{C_2}\right)$$

In the above, m_f^* is mass effect of ER fluid, c_f viscous damping effect of the flow resistance in the electrode in the absence of the electric field, k_1 and k_2 the spring effects of ER damper which represent the compliance effects of the lower, upper, and gas chambers, and F_y the yield force which can be controlled by the electric field intensity. The post-yield force behavior loop is mainly determined by the parameters c_f and F_y. The width, slope, and smoothness of the hysteresis loop in the pre-yield regions are determined by m_f^*, k_1 and k_2. The hysteresis loop shape factor μ is considered to the theoretical mass $m_f(= I_f A_f A_p)$ for the smoothness of the pre-yield hysteresis loop. The evolutionary variable x_r can be obtained from Eq. (9). The excitation displacement x can affect the damping force behavior of the ER damper through the second-order differential equation. The mechanism of the proposed hydraulic model can be expressed by parallel and serial combinations of a spring, a viscous dash-pot, and a Coulomb friction elements as shown in Fig. 3(b). It is noted that the governing equations (8) and (9) well describe the flow motion of the hydraulic ER damper.

4. Assessment of model

In order to minimize the mean square error between the measured and prediction force, the parameter identification has been undertaken. In this work, a constrained least-mean-square

(LMS) error minimization procedure available in the MATLAB is adopted [14]. The cost functions J for the hydro-mechanical model is defined by

$$J(c_f, F_y, k_1, k_2) = \sum_{k=1}^{N} [f(t_k) - \hat{f}(t_k)]^2 \tag{11}$$

where $\hat{f}(t_k)$ is the force calculated using model (8) and (9), $f(t_k)$ the measured force, and t_k the time at which the kth sample has been taken. The parameter $m_f^*(= m_f\mu)$ in Eqs. (8) and (9) is not adopted for the parameter optimization. To get tendencies of the other parameters with respect to the excitation frequencies and electric field intensities, the fixed value of m_f^* is used for the identification of the other parameters. The theoretical calculation of fluid inertia effect results in $m_f = 0.11\,\text{kg}$, and the pre-yield hysteresis loop shape factor μ is tuned to 26.9 by empirical intuition. The four parameters c_f, F_y, k_1, and k_2 are estimated so as to minimize the cost function J. Fig. 4 shows the optimized parameters of c_f, F_y, k_1, and k_2, respectively. It is noted that the stiffness k_2 tends to increase as the electric field intensity increases, and the identified stiffness k_1 is smaller than k_2. It is observed that the optimized parameters have the dependence on the electric

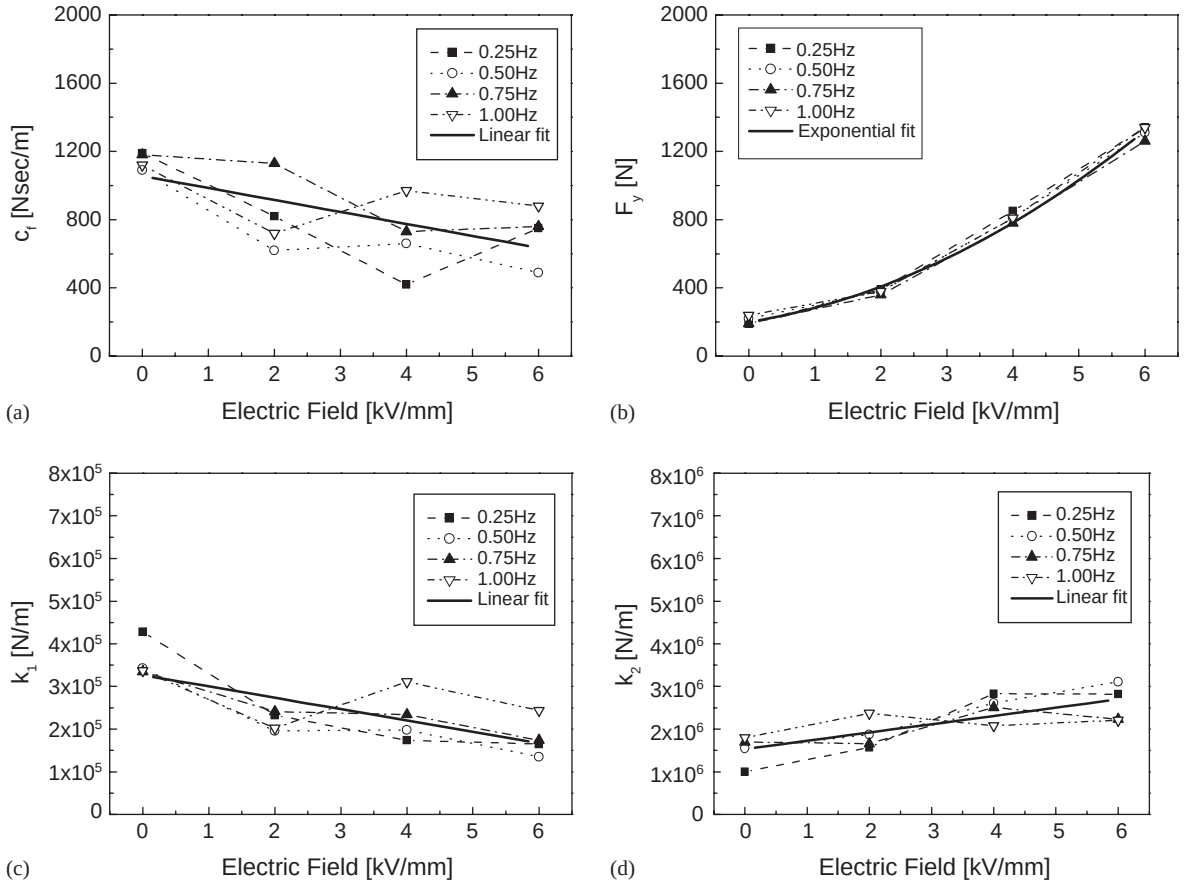

Fig. 4. Identified parameters of the hydro-mechanical model. (a) Damping c_f, (b) yield force F_y, (c) stiffness k_1, (d) stiffness k_2.

field intensity. Thus, arithmetic mean values of parameters (c_f, k_1, k_2) at each frequency are linearized with respect to the input electric field intensity and given as follows: $c_f = 1055 - 70E, k_1 = 326750 - 26625E$, and $k_2 = 1533000 + 194000E$. On the other hand, the yield force F_y is represented by exponential form $F_y = 199.8 + 67.1E^{1.57}$. Thus, the dependence of damping force on the electric field intensity is accounted in the hydro-mechanical model.

Now, the damping force vs. velocity cycles are reconstructed using the parameters obtained from the optimization procedures. The plot is obtained by applying the electric field of 0 and 6 kV/mm at the excitation frequency of 1.0 Hz. For the Bingham model, the comparison of the predicted and measured force vs. velocity is shown in Fig. 5(a). It is obvious that Bingham model cannot capture the pre-yield hysteresis behavior of damping force, although it well represents post-yield force vs. velocity behavior. Fig. 5(b) shows the force vs. velocity hysteresis cycles reconstructed from the hydro-mechanical model with optimized parameters. Fig. 5(c) shows the hysteresis cycles of the hydro-mechanical model with the parameters fitted by electric field intensity. As shown in the figures, the pre-yield hysteresis force behavior is well represented by the lumped mechanical parameters.

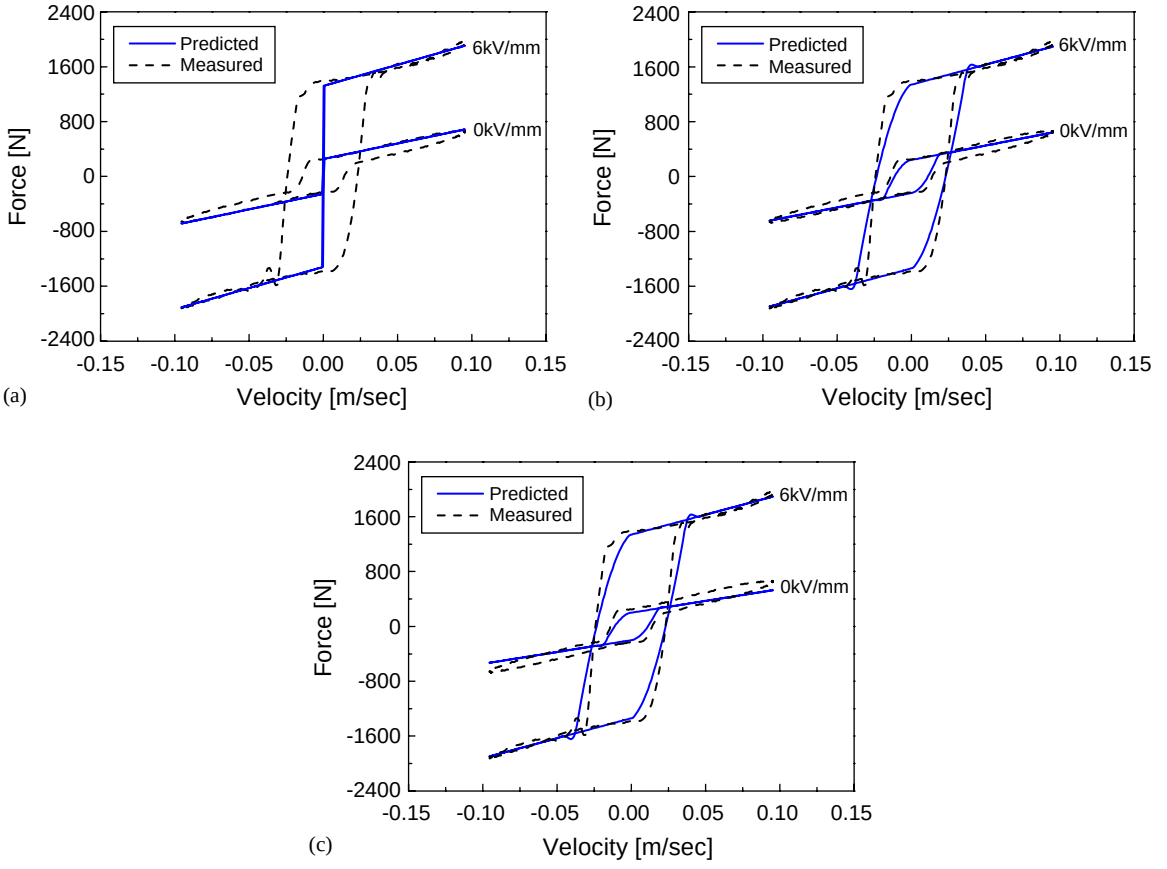

Fig. 5. Comparison of damping forces between the measurement and prediction. (a) Bingham model, (b) hydro-mechanical model with identified parameters, (c) hydro-mechanical model with fitted parameters.

In order to compare model performance in the identified force time history, the averaged error between the modeled and measured force time history is calculated for each model. By calculating the force error, we obtain a quantitative measure of how well each model characterizes the behavior of the ER damper. The relative root mean squared (rms) force error per cycle is defined as follows:

$$\text{Relative rms error} = \frac{[\sum_{k=1}^{m}[f(t_k) - \hat{f}(t_k)]^2]^{1/2}}{[\sum_{k=1}^{m}[f(t_k)]^2]^{1/2}} \times 100. \tag{12}$$

In the above, m is the number of data over one cycle. The rms value of the force error is divided by the rms value of the measured force. Fig. 6 shows the force errors for each model. As expected, the error of the Bingham model is much larger than that of the proposed hydraulic-mechanical model. The damping force prediction error of the hydro-mechanical model with the parameters functionalized by electric field intensity slightly larger than the model with optimally identified parameters. But it is evident that model prediction capability of the hydro-mechanical model with the fitted parameters is much better than the conventional Bingham model.

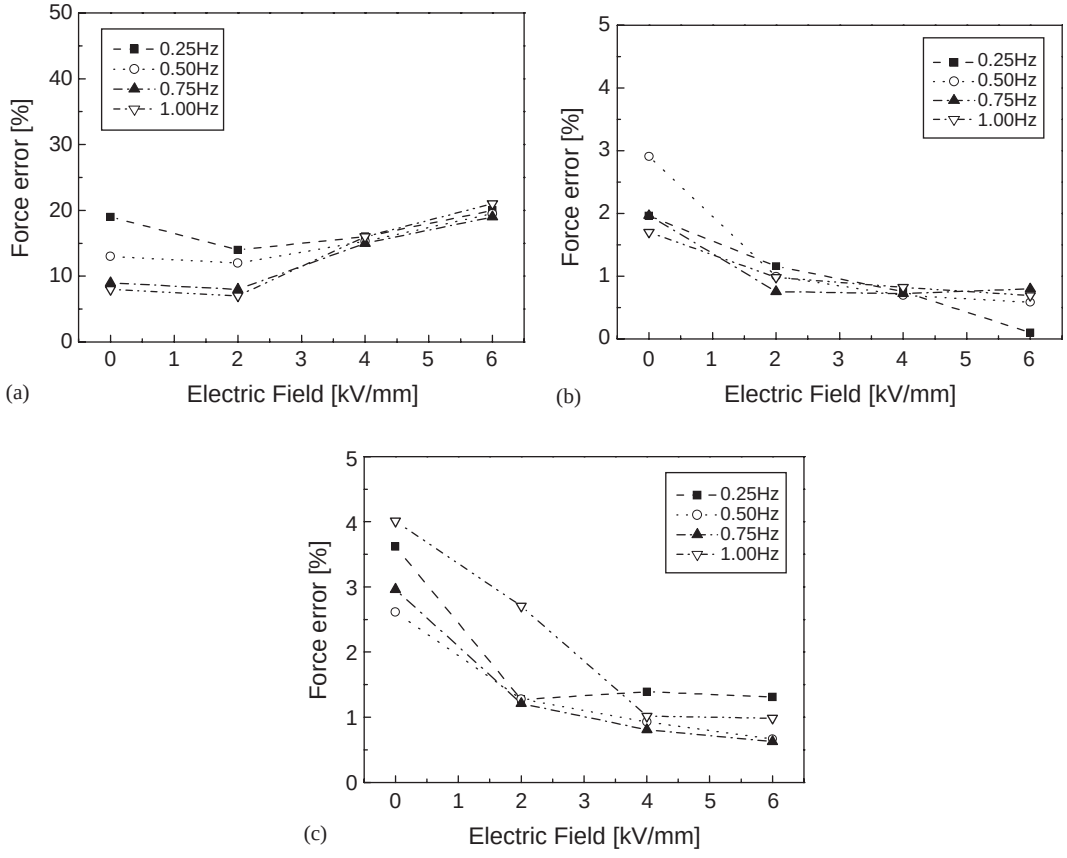

Fig. 6. Relative rms force error for the identification of data sets. (a) Bingham model, (b) hydro-mechanical model with identified parameters, (c) hydro-mechanical model with fitted parameters.

5. Concluding remarks

In this work, a hydro-mechanical model for the prediction of the field-dependent hysteretic damping force of the ER damper was proposed. The model well describes physical flow motion of the hydraulic-type ER damper. In addition, the proposed model can account for the compliance effects manifested in the pre-yield hysteresis characteristics. It has been demonstrated that the hysteretic behavior can be well reconstructed by utilizing the proposed model associated with the optimally identified parameters. It is finally remarked that a feedback control performance of the ER damper using the hydro-mechanical model will be undertaken in the near future.

Acknowledgements

This was supported by the National Research Laboratory (NRL) program directed by Korea Ministry of Science and Technology. This financial support is gratefully acknowledged.

References

[1] R. Stanway, J.L. Sproston, A.K. EI-Wahed, Application of electrorheological fluids in vibration control: a survey, *Smart Materials and Structures* 5 (4) (1996) 464–482.
[2] S.B. Choi, Y.T. Choi, E.G. Chang, S.J. Han, C.S. Kim, Control characteristics of a continuously variable ER damper, *Mechatronics* 8 (1998) 143–161.
[3] S.B. Choi, Y.T. Choi, D.W. Park, A sliding mode control of a full-car electrorheological suspension system via hardware in-the-loop simulation, *Journal of Dynamic Systems, Measurement, and Control* 112 (2000) 114–121.
[4] Y.T. Choi, N.M. Wereley, Y.S. Jeon, Semi-active vibration isolation using magnetorheological isolators, *SPIE's Ninth Annual International Symposium on Smart Structures and Materials*, SPIE Vol. 4697, CA, USA, 2002, pp. 284–291.
[5] R.A. Snyder, G.M. Kamath, N.M. Wereley, Characterization and analysis of magnetorheological damper behavior under sinusoidal loading, *AIAA Journal* 39 (7) (2001) 1240–1253.
[6] G.M. Kamath, M.K. Hurt, N.M. Wereley, Analysis and testing of Bingham plastic behavior in semi-active electrorheological fluid dampers, *Smart Materials and Structures* 5 (1996) 576–590.
[7] Li Pang, G.M. Kamath, N.M. Wereley, Analysis and testing of a linear stroke magnetorheological damper, *AIAA/ASME/AHS Adaptive Structures Forum*, Vol. CP9803, Part 4, CA, USA, 1998, pp. 2841–2856.
[8] N.M. Wereley, Li Pang, G.M. Kamath, Idealized hysteresis modeling of electrorheological and magnetorheological dampers, *Journal of Intelligent Material Systems and Structures* 9 (8) (1998) 642–649.
[9] G.M. Kamath, N.M. Wereley, Nonlinear viscoelastic-plastic mechanism-based model of an electrorheological damper, *Journal of Guidance, Control, and Dynamics* 20 (6) (1997) 1125–1132.
[10] B.F. Spencer, S.J. Dyke, M.K. Sain, J.D. Carlson, Phenomenological model of a magnetorheological damper, *Journal of Engineering Mechanics* 123 (3) (1997) 230–238.
[11] S.J. Dyke, B.F. Spencer Jr., M.K. Sain, J.D. Carlson, Modeling and control of magnetorheological dampers for seismic response reduction, *Smart Materials and Structures* 5 (5) (1996) 565–575.
[12] S.B. Choi, S.K. Lee, Y.P. Park, A hysteresis model for the field-dependent damping force of a magnetorheological damper, *Journal of Sound and Vibration* 245 (2) (2001) 375–383.
[13] R. Singh, G. Kim, P.V. Pavindra, Linear analysis of automotive hydro-mechanical mount with emphasis on decoupler characteristics, *Journal of Sound and Vibration* 158 (2) (1992) 219–243.
[14] MATLAB Optimization Toolbox, The Math Works, Inc., Natick, MA, 1996.